Supporting Information

Ionic liquid-induced in-situ deposition of perovskite quantum dot films with photoluminescence quantum yield over 85%

Qiugui Zeng,[a,b] Xin Luo,[a,b] Yiying Du,[b] Jiexuan Jiang,[a,b] Lin Yang,[c] Hui Zhao,[c] Heping Shi,[d] Yanbo Li [a,b,*]

[a]Yangtza Delta Region Institute (Huzhou), University of Electronic Science and Technology of China, Huzhou 313001, China

[b]Institute of Fundamental and Frontier Sciences, University of Electronic Science and Technology of China, Chengdu 610054, China

[c]School of Chemical Engineering, Sichuan University, Chengdu 610065, China

[d]School of Chemistry and Chemical Engineering, Shanxi University, Taiyuan 030006, China

[*]Corresponding Author: yanboli@uestc.edu.cn

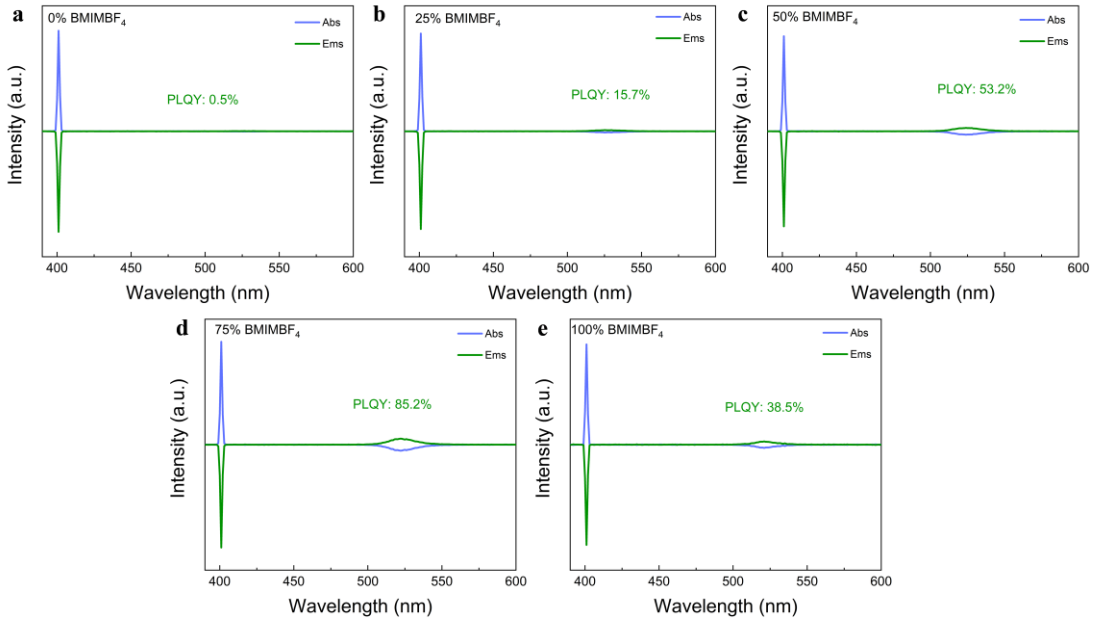

Fig. S1 Absolute PLQY measurement of polycrystalline perovskite film (a), 25% $BMIMBF_4$-induced QD film (b), 50% $BMIMBF_4$-induced QD film (c), 75% $BMIMBF_4$-induced QD film (d) and 100% $BMIMBF_4$-induced QD film (e).

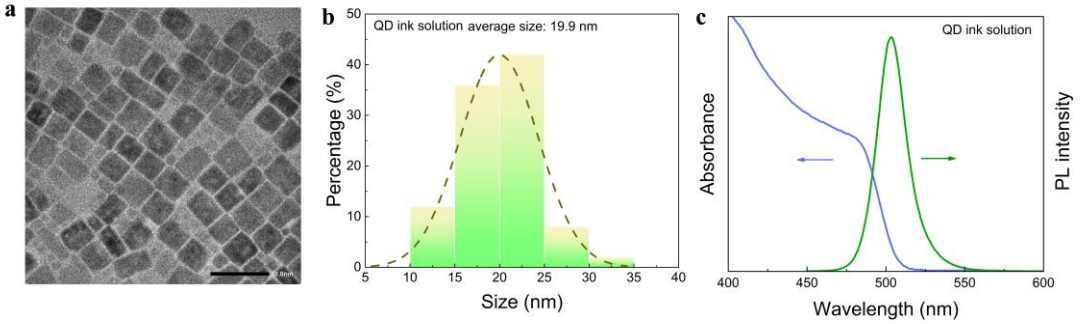

Fig. S2 (a) TEM image of conventional $CsPbBr_3$ QD ink solution. (b) Histogram of QD size in a. (c) Absorption and PL spectra of conventional $CsPbBr_3$ QD ink solution.

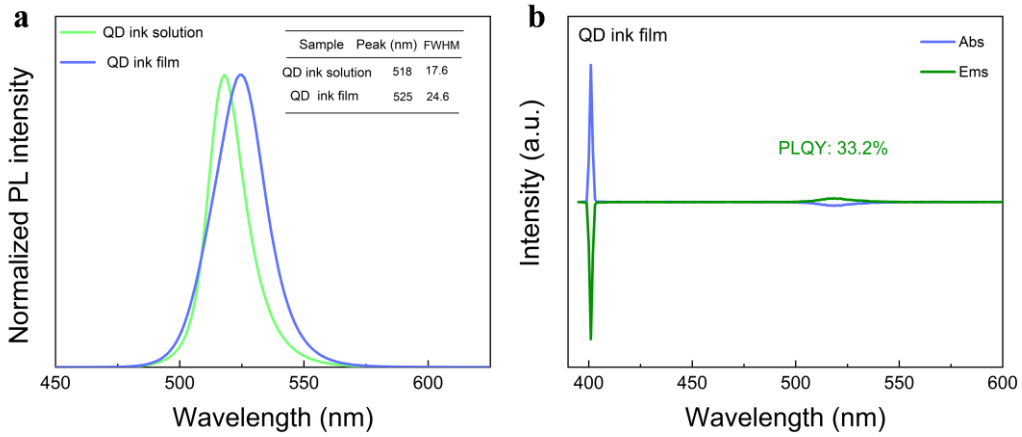

Fig. S3 (a) Normalized PL spectra of QD ink solution and consequently deposited QD ink film. (b) Absolute PLQY measurement of the conventional QD ink film.

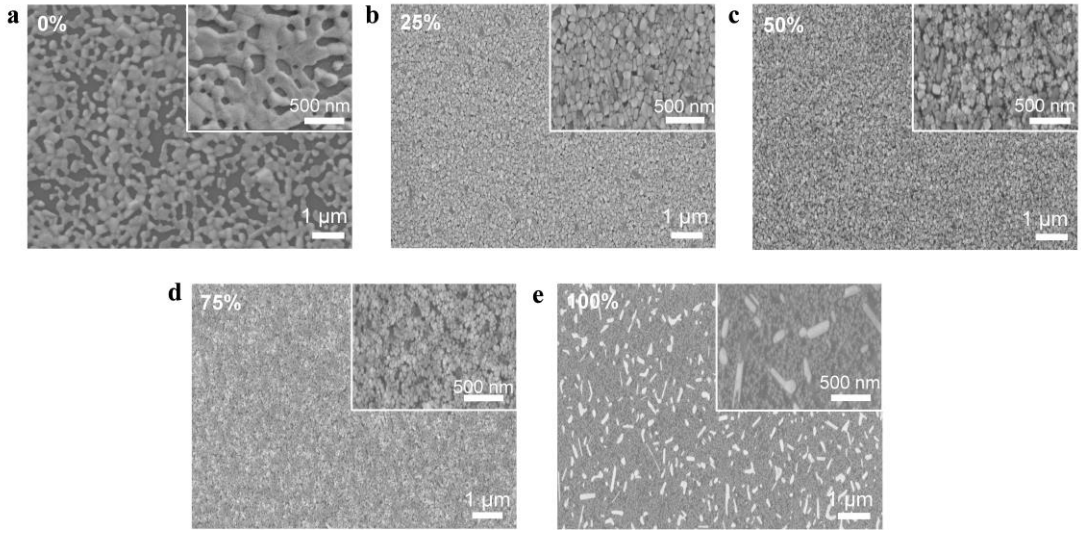

Fig. S4 SEM images of the polycrystalline perovskite film (a), 25% $BMIMBF_4$-induced QD film (b), 50% $BMIMBF_4$-induced QD film (c), 75% $BMIMBF_4$-induced QD film (d), and 100% $BMIMBF_4$-induced QD film (e). The inset in a-e show high-magnification SEM images of the respective sample.

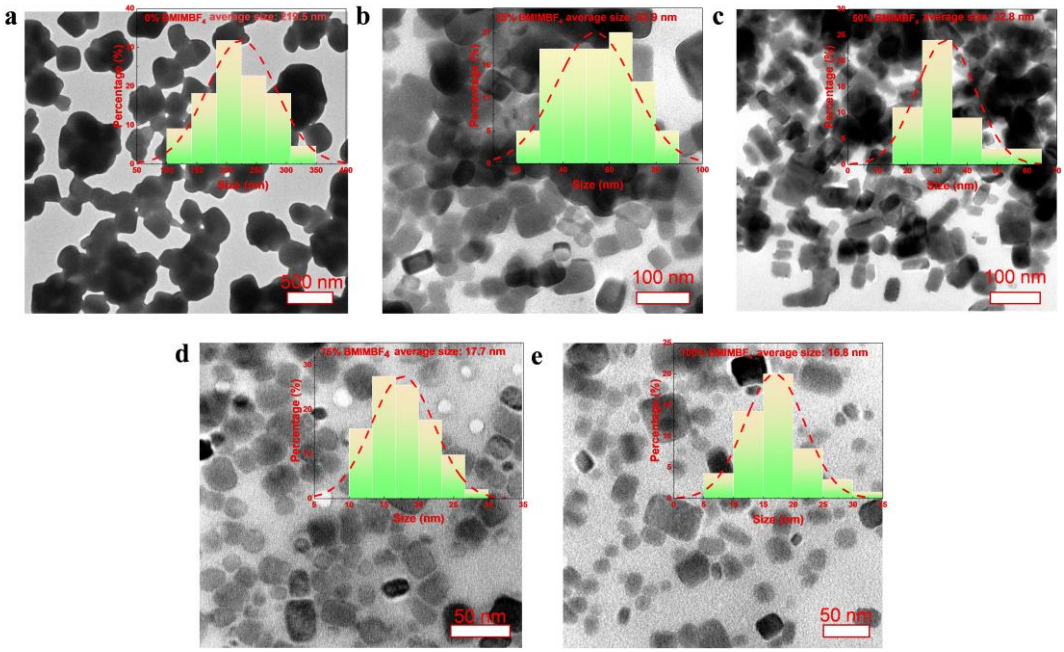

Fig. S5 TEM images of the polycrystalline perovskite sample (a), 25% $BMIMBF_4$-induced QD sample (b), 50% $BMIMBF_4$-induced QD sample (c), 75% $BMIMBF_4$-induced QD sample (d) and100% $BMIMBF_4$-induced QD sample. The insets in a-e show the histogram of grain/QD size for the respective sample.

Fig. S6 The photograph of CsBr·DMSO, $PbBr_2$·DMSO, CsBr·$BMIMBF_4$·DMSO, $PbBr_2$·$BMIMBF_4$·DMSO and $BMIMBF_4$·DMSO solutions. The red circle marks the undissolved CsBr in DMSO.

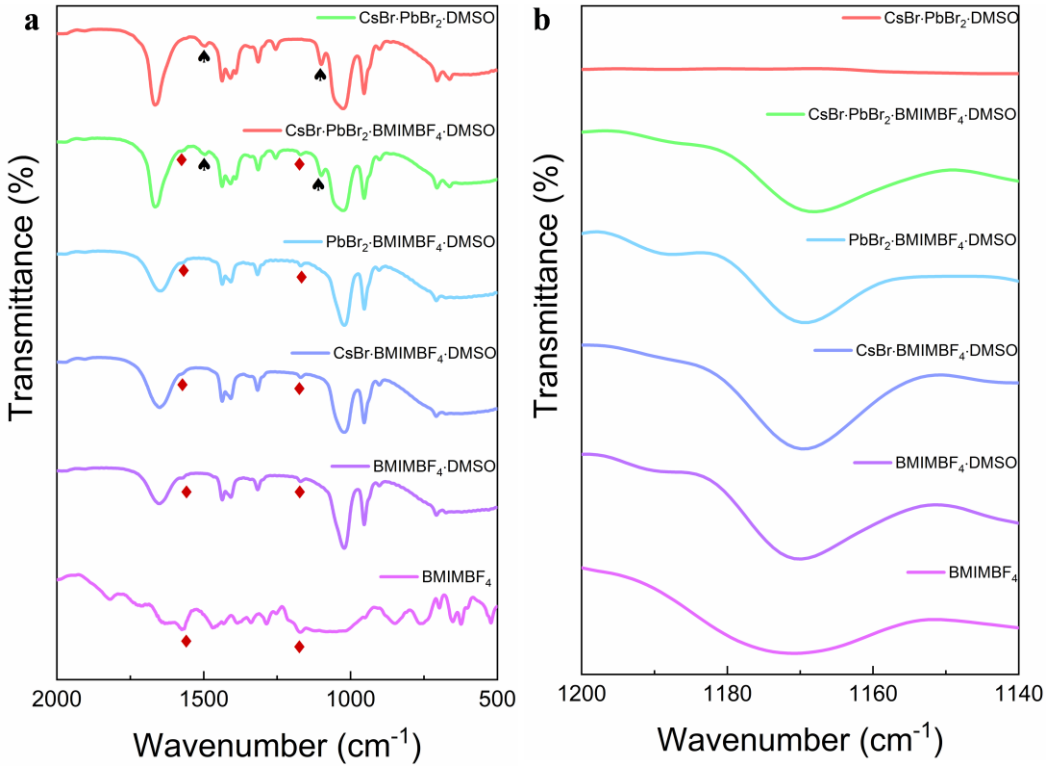

Fig. S7 (a) FTIR spectra of CsBr•DMSO, $PbBr_2$•DMSO, CsBr•$BMIMBF_4$•DMSO, $PbBr_2$ • $BMIMBF_4$ • DMSO and $BMIMBF_4$ • DMSO solutions. The red rectangles represent the characteristic peaks of $BMIMBF_4$ ionic liquid, the spades represent the characteristic peaks of perovskite precursor. (b) The magnification of a in the range of 1200 cm^{-1} to 1140 cm^{-1}.

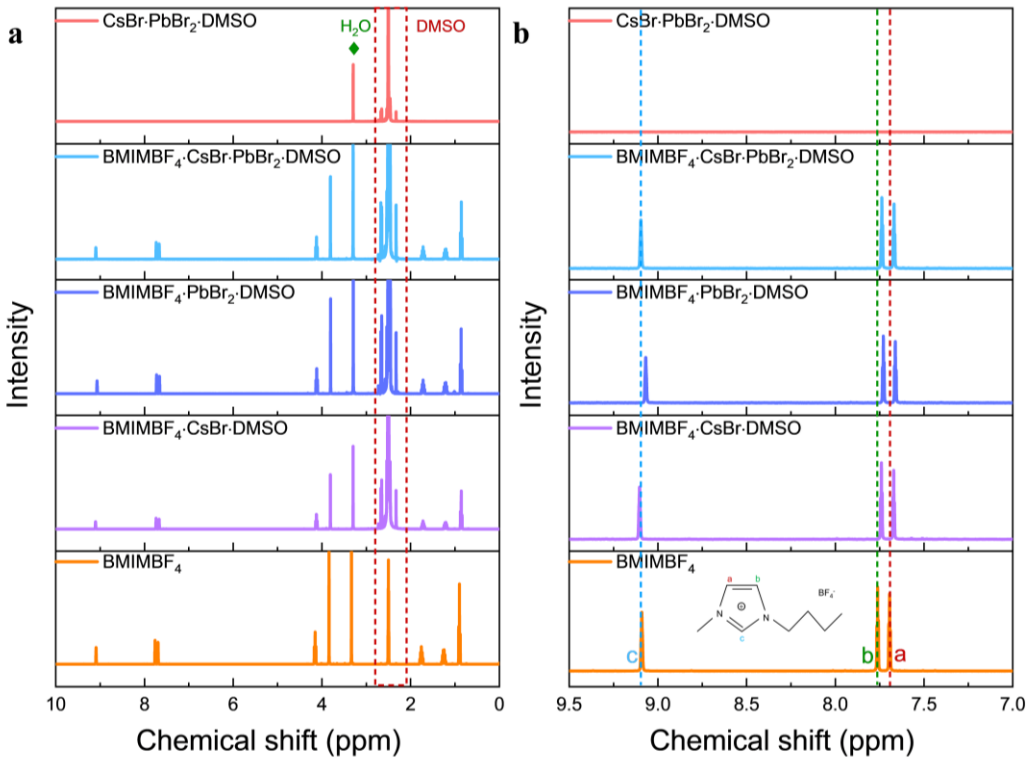

Fig. S8 (a) ^{1}H NMR spectra of the $BMIMBF_4$, $BMIMBF_4$•CsBr•DMSO, $BMIMBF_4$•$PbBr_2$•DMSO, $BMIMBF_4$•CsBr•$PbBr_2$•DMSO, CsBr•$PbBr_2$•DMSO samples in the dimethyl sulfoxide-d_6. (b) The magnification of a in the range of 9.5 to7.0 ppm, the inset shows the structure of the $BMIMBF_4$.

As shown in Fig. S8, the butyl chain (-CH) attached on imidazolium ring in the range from 1.76 to 0.88 ppm remain unchanged in the $BMIMBF_4$-contained samples and the features originated from the a-CH and b-CH of imidazolium ring show higher upfield shift in the $BMIMBF_4$•CsBr•DMSO, $BMIMBF_4$•$PbBr_2$•DMSO, $BMIMBF_4$•CsBr•$PbBr_2$•DMSO samples. This result indicates the presence of the high shield effect in the a-CH and b-CH of imidazolium ring for $BMIMBF_4$•CsBr•DMSO, $BMIMBF_4$•$PbBr_2$•DMSO, $BMIMBF_4$•CsBr•$PbBr_2$•DMSO samples, due to the interaction between the acidic hydrogen from imidazolium ring and electronegative halides. Besides, we noticed that the c-CH of imidazolium ring had no or slight shift in the $BMIMBF_4$-contained samples, these results demonstrate that the a-CH and b-CH of imidazolium ring prefer to interact with the electronegative halides other than the c-CH of imidazolium ring. Therefore, we conclude that the ^{1}H NMR results are consistent with the FTIR results

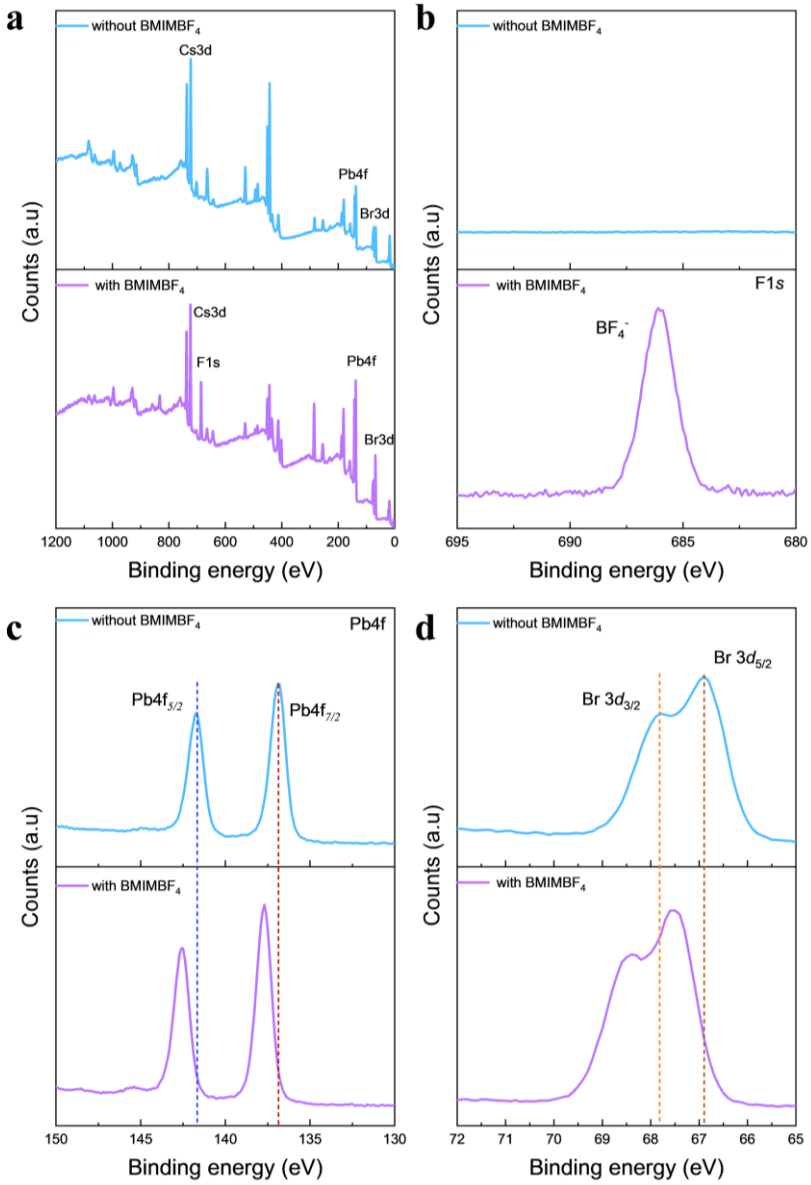

Fig. S9 XPS spectra of the polycrystalline perovskite film (without $BMIMBF_4$ IL) and 75% $BMIMBF_4$-induced perovskite QD film (with $BMIMBF_4$ IL), (a)survey, (b) F 1s, (c) Pb 4f and (d) Br 3d.

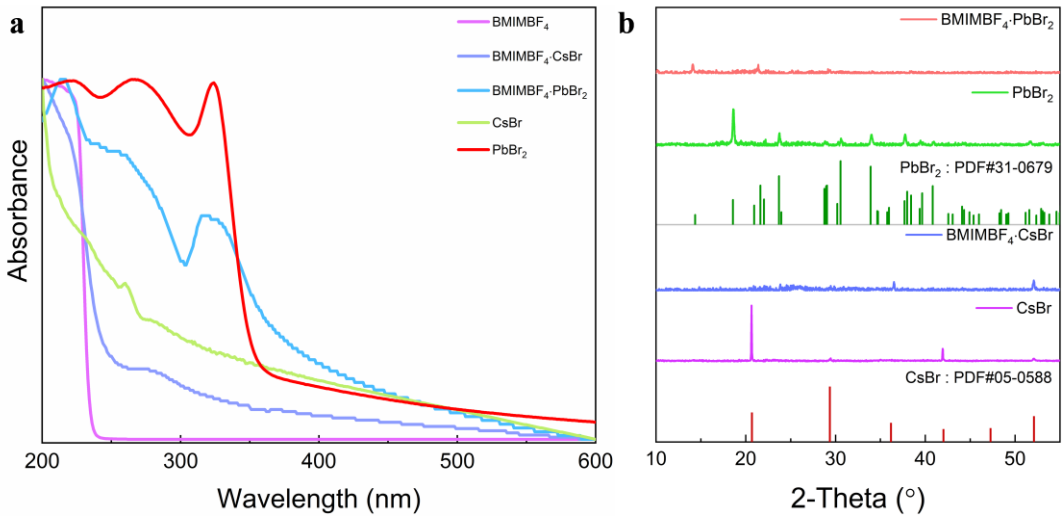

Fig. S10 (a) Absorption spectra of CsBr, $PbBr_2$, $BMIMBF_4$•$PbBr_2$, $BMIMBF_4$•CsBr films and $BMIMBF_4$ ionic liquid. (b) XRD patterns of CsBr, $PbBr_2$, $BMIMBF_4$•$PbBr_2$ and $BMIMBF_4$•CsBr film.

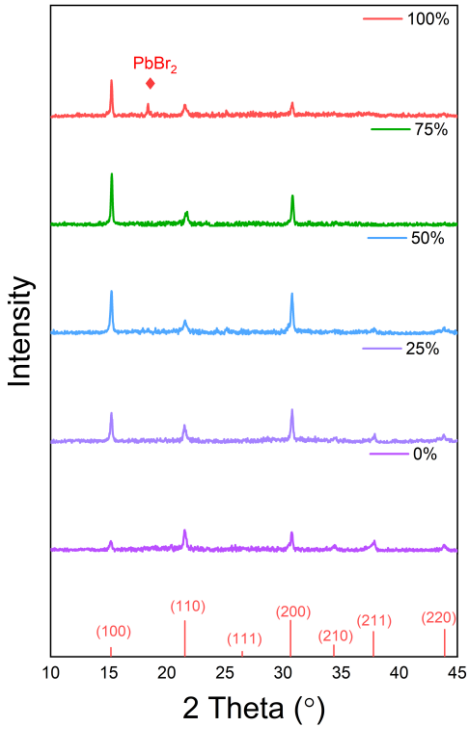

Fig. S11 XRD patterns of samples with different $BMIMBF_4$ concentrations (from 0% to 100%).

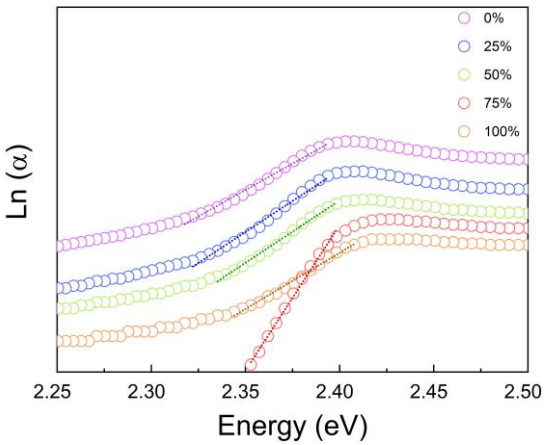

Fig. S12 Ln (α) vs photon energy for samples with different $BMIMBF_4$ concentrations. The E_u values are obtained from the slope of the fitted curves.

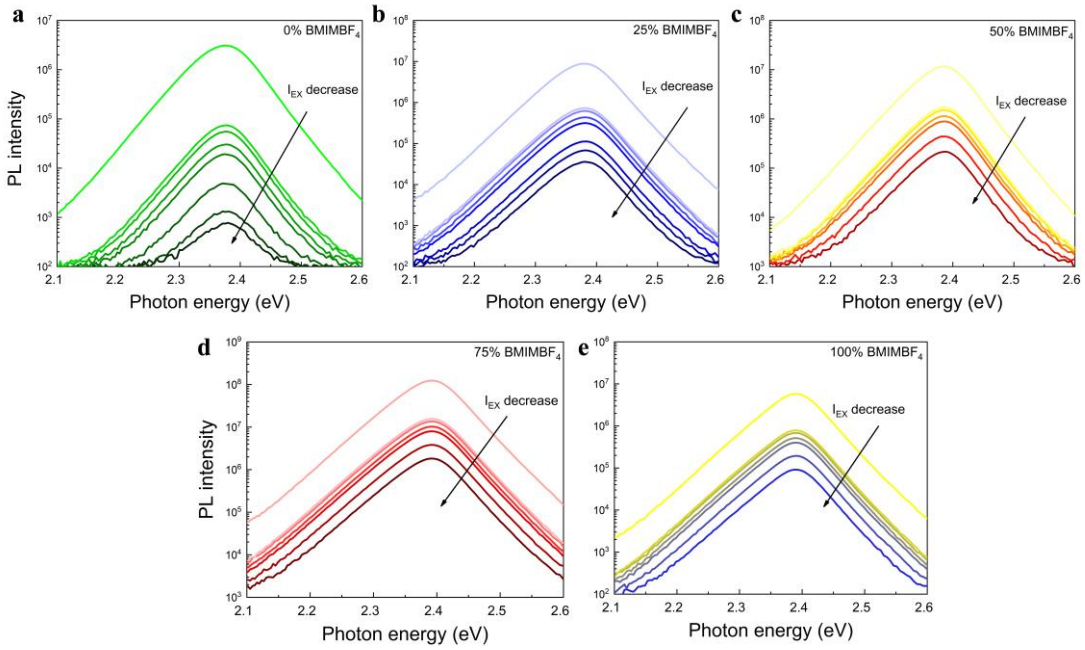

Fig. S13 PL spectra recorded with excitation density from 1.32 mW/cm^2 to 98.43 mW/cm^2 for 0% $BMIMBF_4$-induced QD film (a), 25% $BMIMBF_4$-induced QD film (b), 50% $BMIMBF_4$-induced QD film (c), 75% $BMIMBF_4$-induced QD film (d) and 100% $BMIMBF_4$-induced QD film (e).

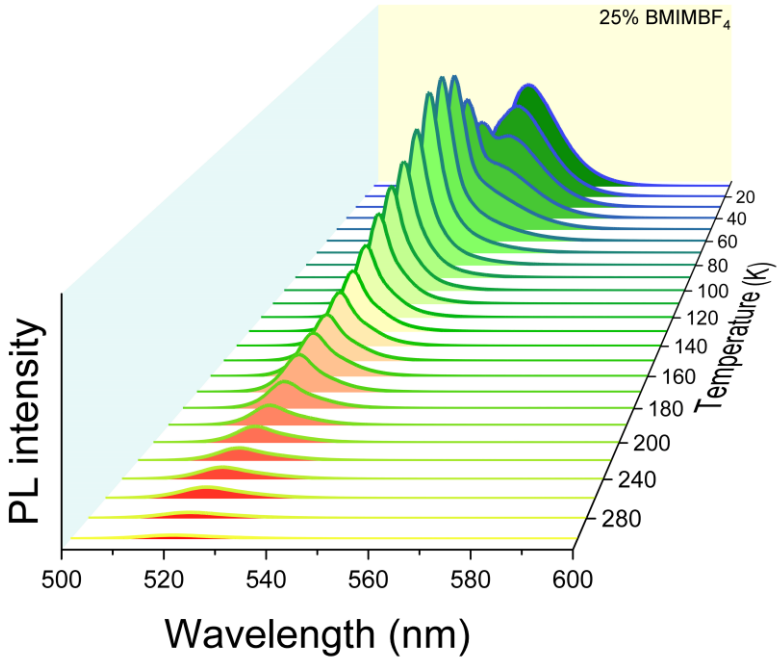

Fig. S14 Temperature-dependent PL spectra of the 25% $BMIMBF_4$-induced QD film in the range of 10 to 300 K.

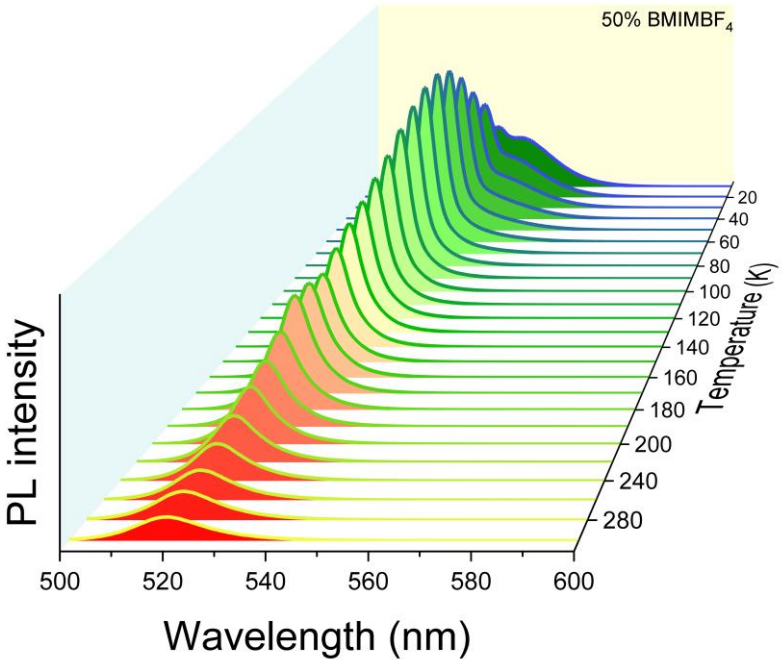

Fig. S15 Temperature-dependent PL spectra of the 50% $BMIMBF_4$-induced QD film in the range of 10 to 300 K.

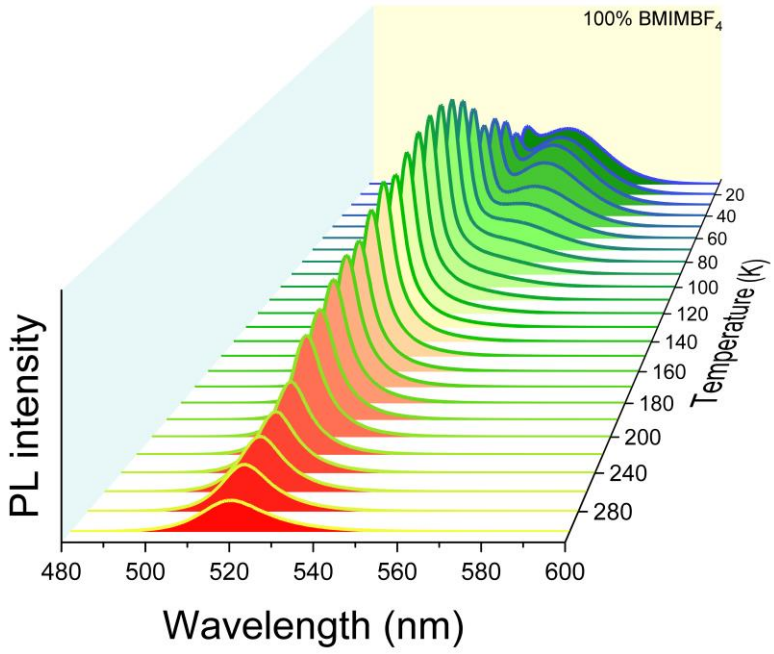

Fig. S16 Temperature-dependent PL spectra of the 100% $BMIMBF_4$-induced QD film in the range of 10 to 300 K.

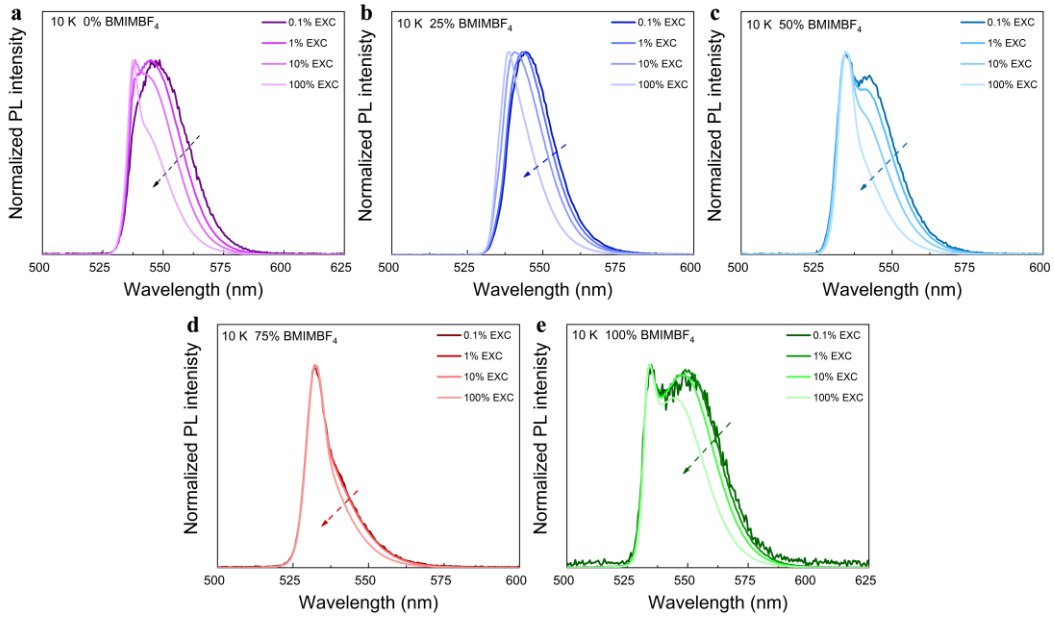

Fig. S17 Normalized PL spectra measured under different excitation intensity at 10 K for the polycrystalline perovskite film (a), 25% $BMIMBF_4$-induced QD film (b), 50% $BMIMBF_4$-induced QD film (c), 75% $BMIMBF_4$-induced QD film (d) and 100%

$BMIMBF_4$-induced QD film (e).The actual laser intensities under different neutral density filters (0.1-100%) are measured to be 0.19 mW/cm^2 (0.1%), 1.32 mW/cm^2 (1%), 11.86 mW/cm^2 (10%), and 98.43 mW/m^2 (100%).

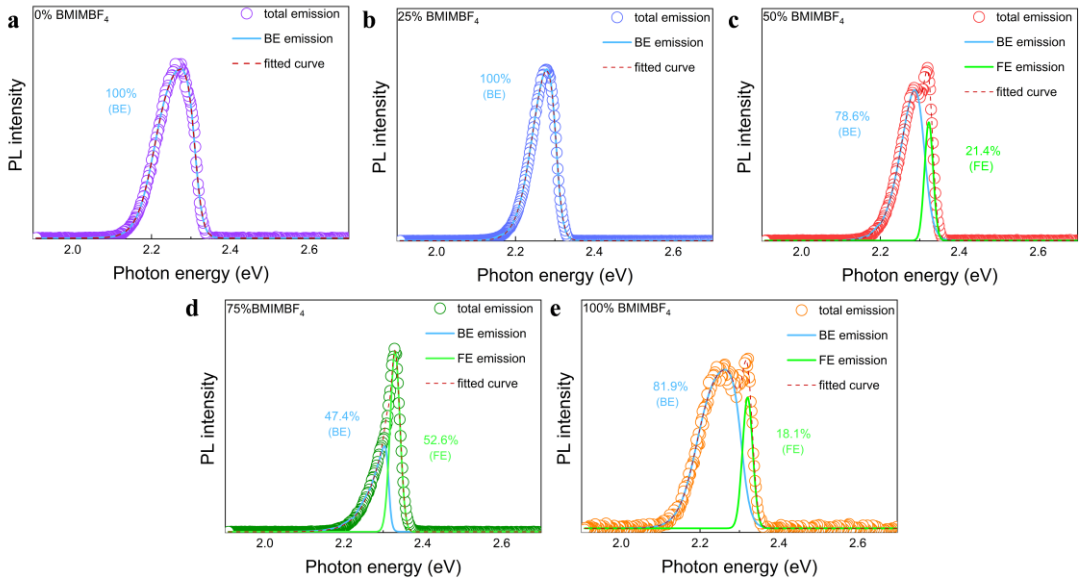

Fig. S18 Peak fittings for low-temperature PL spectra measured at 10 K under a laser intensity of 0.19 mW/cm^2 for the polycrystalline perovskite film (a), 25% $BMIMBF_4$-induced QD film (b), 50% $BMIMBF_4$-induced QD film (c), 75% $BMIMBF_4$-induced QD film (d) and 100% $BMIMBF_4$-induced QD films (e).

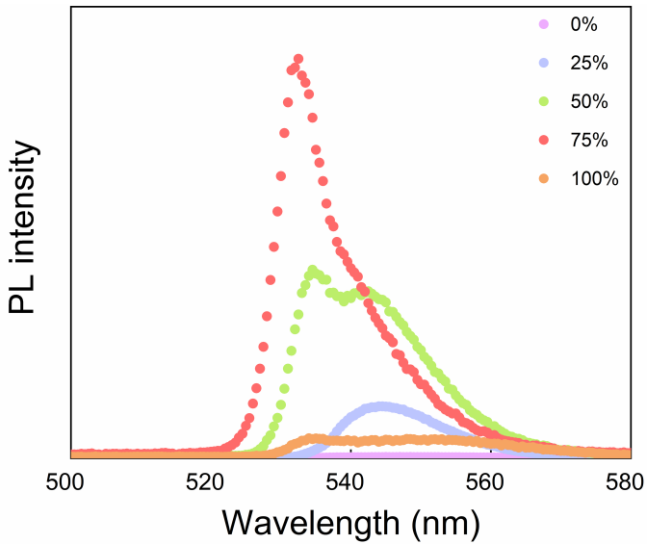

Fig. S19 Low temperature PL spectra of samples with different $BMIMBF_4$ concentrations (from 0 to 100%) at 10 K under a laser intensity of 0.19 mW/cm^2.

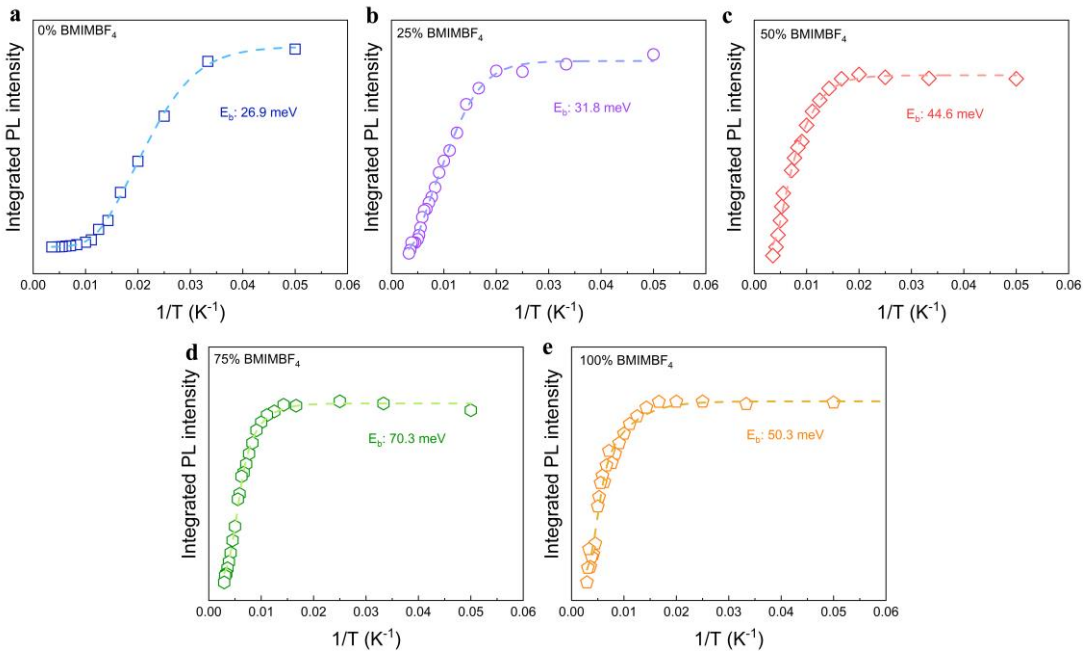

Fig. S20 Integrated PL intensity vs inverse of temperature for the polycrystalline perovskite (a), 25% $BMIMBF_4$-induced QD film (b), 50% $BMIMBF_4$-induced QD film (c), 75% $BMIMBF_4$-induced QD film (d) and 100% $BMIMBF_4$-induced QD films (e). The curves are fitted by Arrhenius equation to obtain the E_b values.

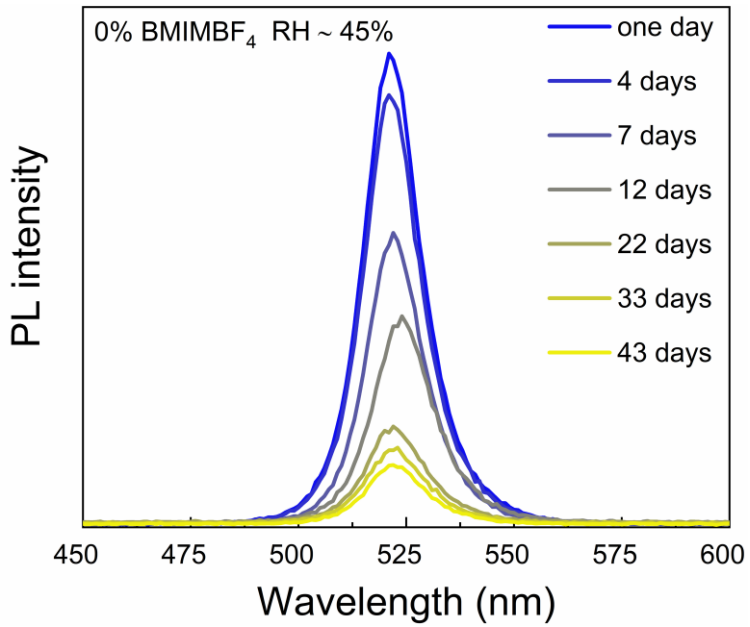

Fig. S21 Temporal evolution of PL spectra of the polycrystalline perovskite film stored in air with RH around 45%.

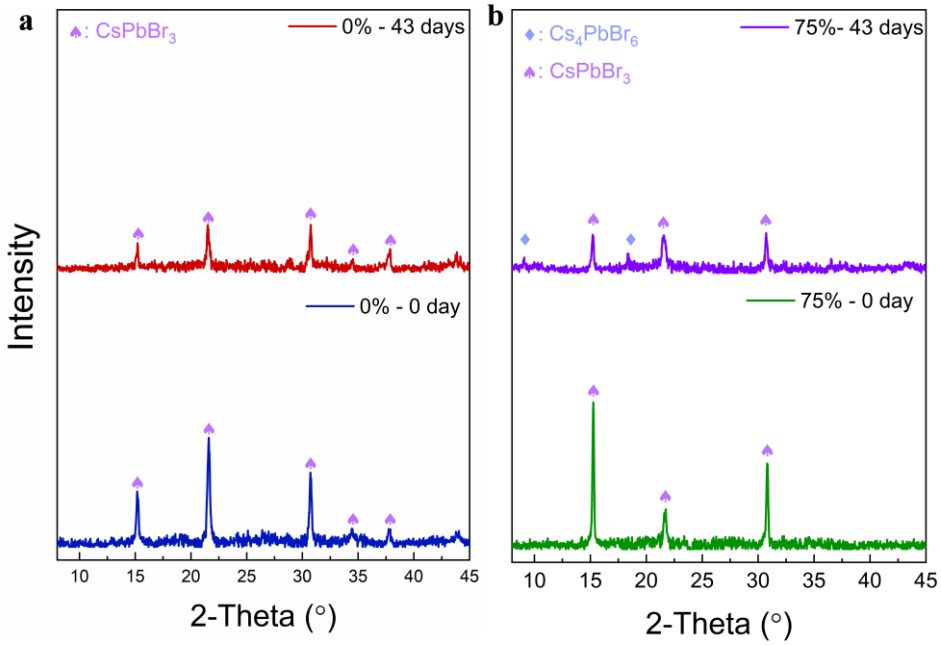

Fig. S22 XRD patterns of samples exposed to air for 0 day and 43 days for the polycrystalline perovskite film (a) and the 75% $BMIMBF_4$-induced QD film (b).

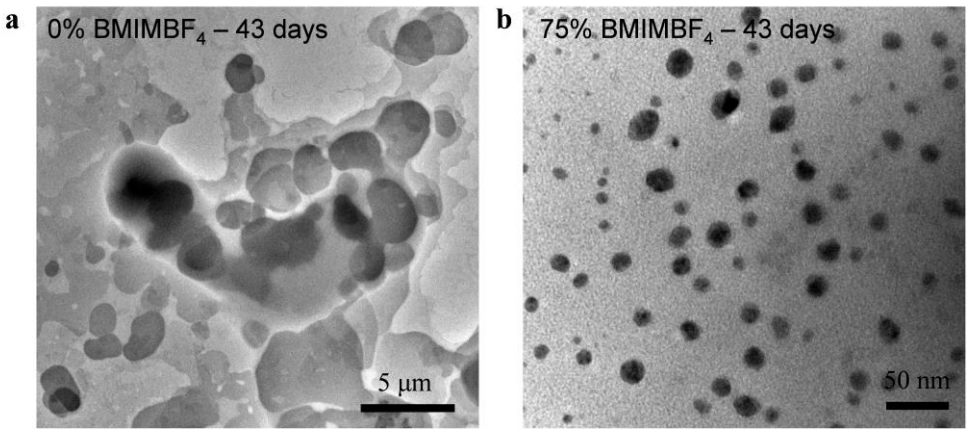

Fig. S23 TEM images of samples exposed to air for 43 days: (a) the polycrystalline perovskite sample, (b) the 75% $BMIMBF_4$-induced QD sample.

Table S1. Fitting parameters of TRPL decay curves and the calculated average lifetimes.

Sample	τ_{free}	A_{free}	τ_{bound}	A_{bound}	β	$<\tau_{bound}>$ (ns)	$<\tau>$ (ns)
0%	12.28	0.02	0.89	0.98	0.435	2.39	3.3
25%	11.05	0.20	38.45	0.80	0.462	89.97	87.6
50%	5.37	0.21	29.40	0.79	0.494	60.14	58.9
75%	3.98	0.22	20.87	0.78	0.597	31.64	30.7
100%	4.99	0.18	25.76	0.82	0.600	38.76	37.8

Note: the TRPL decay curve is fitted by the thermalized stretching exponential decay:[1]

$$I = A_{free}\, exp\left(-\frac{t}{\tau_{free}}\right) + A_{bound}\, exp\left(-\left(\frac{t}{\tau_{bound}}\right)^{\beta}\right)$$

The average lifetime of the stretched exponential decay $<\tau_{bound}>$ is obtained according to the following equation:

$$<\tau>=\frac{\tau_{bound}}{\beta} * \Gamma(\frac{1}{\beta})$$

where $\Gamma\left(\frac{1}{\beta}\right)$ is the gamma function.[2, 3]

The total average lifetime of time-resolved PL decay curve is obtained according to the following equation:

$$<\tau>=\frac{I_1 * \tau_1^2 + I_2 *<\tau_2>^2}{I_1 * \tau_1 + I_2 *<\tau_2>}$$

References

1 H. He; Q. Yu; H. Li; J. Li, J. Si, Y. Jin, N. Wang, J. Wang, J. He, X. Wang, Y. Zhang and Z. Ye, Exciton Localization in Solution-Processed Organolead Trihalide Perovskites, *Nat. Commun.*, 2016**, 7**, 10896.

2 C. P. Lindsey and G. D. Patterson, Detailed Comparison of the Williams–Watts and Cole–Davidson Functions, *J. Che. Phys.*, 1980, **73**, 3348-3357.

3 D. W. deQuilettes, S. Koch, S. Burke, R. K. Paranji, A. J. Shropshire, M. E. Ziffer, D. S. Ginger, Photoluminescence Lifetimes Exceeding 8 μs and Quantum Yields Exceeding 30% in Hybrid Perovskite Thin Films by Ligand Passivation, *ACS Energy Lett.*, 2016**, 1**, 438-444.